



Gas sorption-induced pore radius change and their impact on gas apparent permeability

Asadullah Memon¹ · Aifen Li¹ · Muhammad Kashif² · Nangendo Jacqueline¹

Received: 27 May 2020 / Accepted: 19 November 2020 / Published online: 1 December 2020

© Springer Nature Switzerland AG 2020

Abstract

Shale gas reservoirs contain small pore network that typically range from macro to nano meters and abundant gas storage as sorbed gas. In addition, the storage medium in such pore network varies and may be affected by physical parameters of shale matrix. This work presents the influence of gas sorption on pore radius and thickness at low and high pressure and analyzes the gas apparent permeability. Langmuir model is generally used to quantify the adsorbed layer thickness; however, such model undertakes mono-layer gas sorption on pore surfaces and provides poor results especially at high pressure. In this work, supercritical dubinin radushkevich (SDR) model, micropore-filling mechanism based, has been used to quantify the adsorbed layer thickness and their results have been compared with Langmuir model. The impact of adsorbed gas density on gas sorption and the impact of gas sorption crucial factors on pore radius were examined. At the end, gas slippage, geo-mechanical and adsorbed layers impacts were analyzed for evolution of gas apparent permeability. The proposed gas apparent permeability model was also validated with experimental data. The results show that assumed adsorbed gas density in Langmuir model is misleading the accurate measurement of gas sorption. The SDR model does not only provide an accurate adsorbed gas density but also its values are very close to the experimental at both low and high pressure. Gas sorption-induced pore radius based on SDR model was altered when gas sorption behavior alter at same pressure than Langmuir model-based. Gas apparent permeability changes due to gas slippage, geo-mechanical and gas adsorbed layers impacts. High gas adsorbed layer impact was observed when using proposed model as compared with Langmuir model especially at high pressure.

Keywords Gas sorption · Gas slippage · Geo-mechanical · Adsorbed layer · Gas apparent permeability

1 Introduction

In shale gas reservoirs (SGR) the gas usually flows through a network of several pores and transportations. Gas transport processes are very complex and comprising three important systems [36] such as kerogen, matrix and natural-hydraulic fracture system. All these systems are controlled by various key factors such as pore network characteristics, permeating fluid, pressure, temperature and stress [6] and [23, 24]. The kerogen system includes

organic material which mostly contains micropores (less than 2 nm) and mesopores (2–50 nm) and huge intersected nanopores which offer active places for gas sorption [19]. Organic nanopores provide a place for huge gas storage and contribute significantly more than 50% of total gas storage as adsorbed and absorbed gases, while other storage is free gas [27]. The matrix system includes both organic matter and inorganic matrix, i.e., clay minerals and both have different transport mechanisms and gas sorption capacity [39]. The fracture systems are often

✉ Aifen Li, aifenli@upc.edu.cn | ¹School of Petroleum Engineering, China University of Petroleum (East China), Huangdao district, Qingdao 266580, Shangdong Province, People's Republic of China. ²College of Chemistry, Chemical Engineering and Biotechnology, Donghua University, Shanghai 201620, People's Republic of China.



complicated due to interchange of natural fracture with hydraulic fractures network. Generally in SGR, the gas is desorbing from kerogen, i.e., pore wall and flow towards the matrix system. Then, due to pressure gradient the flux transfer occurs between the matrix and fracture system and gas reaches at the well bore and finally produced. Several transport mechanisms occur in SGR such as viscous, slip, diffusion and gas adsorption and gas desorption [7, 13, 17, 28] and all depend on Knudsen number. The pore size may affect the Knudsen number [22]. The larger average pore diameter may be the cause of smaller Knudsen number and resultant gas flow mechanism differs. In addition, the pore size and thickness may also be affected due to gas sorption and result change of pore volume, porosity and gas permeability.

Gas apparent permeability is a significant factor to characterize the shale gas productivity [9, 10] and [43] and related to Knudsen number. Gas apparent permeability can be measured by following three methods, (a) laboratory experiment, (b) numerical methods and (c) analytical method. Steady-state flow experiment and pulse-decay are common methods used at laboratory; however, such methods are very complex and time consuming due to ultra-low porosity and extremely low permeability of shale rock [9, 10, 45]. Similarly, numerical methods are also widely used, but it also requires large computational resources and time [31, 45]. An analytical method is formulated model under reasonable assumptions [38] and has widely been used nowadays due to its simplicity, accuracy and saving time. Much research has been done to examine the gas apparent permeability, but not enough attention has been paid to adsorbed layer impact especially at high pressure on gas apparent permeability. However, pore radius and their thickness play a vital role in shale gas productivity. For example, Guo et al. [13] showed that change in gas sorption, gas permeability, gas viscosity and pore radius have great impact on gas production. Wei et al. [37] discussed the relationship in between the nanopore radius and thickness of the adsorbed layer. Moghaddam and Jamiolahmady [26] analyzed the combined impacts of gas slippage and geo-mechanics on gas permeability. Wang and Porcu [35] and Huang et al. [15] developed gas apparent permeability model and measured the thickness of the gas adsorption layer-based on Langmuir model.

Since decades the Langmuir isotherm model has generally been used to quantify the gas adsorption of shale reservoirs and undertakes mono-layer gas sorption on pore surfaces [8]. But, some time, it may not provide positive results especially when shale has rich organic carbon and also underestimates the impact of adsorbed layer thickness [30, 37, 41]. The multi-molecular layer adsorption on pore surfaces has been identified by many researchers in shale and gas adsorbed on such multi molecular layer at

both low and high pressure. In this type of adsorption, the SDR model can be best suited as it is based on micropore-filling mechanism. This model is more suitable in term of mathematical and physical success, and may provide better results than Langmuir model at both low and high pressure [29]. Furthermore, this model has a broad application under reservoir conditions because of these key features, (a) wide pressure and temperature ranges, (b) undertakes both mono-layer and multilayer gas sorption, (c) based on micropore-filling mechanism (d) accurate adsorbed phase gas density measurement, and (e) analyses the gas adsorption capacity with depth.

The main goal of this work is to quantify the adsorbed layer thickness and revisit on gas apparent permeability model for SGR. In order to accomplish such goal, following steps were taken: (a) two shale samples were collected and their characteristics analyzed (b) some experimental data were collected from literature sources for model validation and comparison, (c) quantified the adsorbed layer thickness using Langmuir and SDR models and compared their results, (d) investigated the impacts of gas sorption parameters on pore radius and (e) analyzed the gas slippage, geo-mechanical and adsorbed layer thickness using existing and proposed gas apparent permeability model.

2 Experiments and methods

2.1 Sample descriptions

Two intact shale samples were taken from China Petroleum & Chemical Corporation (SINOPEC) and then analyzed the gas sorption capacity and total organic carbon (TOC) at the laboratory. The crush samples with mesh size 40–80 were used for above analysis. The TOC of shale samples 3-124 and 3-153 was 3.66 wt% and 2.94 wt%, respectively.

2.2 Isotherm gas sorption tests

The computer controlled automatic isothermal sorption measuring instrument made by Beijing Yong Rui Da Electronics Co., Ltd (China) was used. The following experimental steps were followed in measuring the isothermal gas sorption experiments: (a) sample crushing and screening, (b) crush the sample drying and water balance and (c) isothermal gas sorption experiments. The details of these steps are given below:

2.2.1 Sample crushing and screening

A large rock was broken into small pieces with the help of hammer and other blunt. Then, an artificial grinding method was used to get 40–80 fine particles; and other

non-rock debris were removed. The other tools used in grinding method are grinding pestles, screens and tweezers.

2.2.2 Crush the sample drying and water balance

Since the moisture content of the sample seriously impacts on gas sorption, the water balance of the sample was carried out before the gas sorption experiment. In this step, the sample was placed in the oven and the oven temperature was set at 120 °C. Then, after 5–6 h of prolonged drying, the water was completely removed from sample. After that dried sample was placed in a desiccator vessel and stored.

2.2.3 Isothermal gas sorption

Under the control of the computer control software, the isothermal gas sorption host was automatically achieved in the entire sorption process, however, during the experiment the pressure boost and vacuum extraction process was done manually (Fig. 1). The crushed samples with the mesh size of 40–80 were selected and used for isothermal gas sorption experiments at 0–9.535 MPa and temperature of 45 °C. The experimental steps that were followed are: (a) clicked to start the experiment and open the device, (b) opened the valves 2, 5, 6 and 7 for reference and experiment cell pressure sensor correction, (c) load the crushed sample, (d) after opening the valves 3, 4, 5, 6 and 7 to vent the gas, the valve 4 was closed, the valve 3 was opened, and the vacuum was applied, (e) after the vacuum was drawn, the valves 3, 5, 6 and 7 were closed, and (f) fill the methane gas into reference cell and then, same gas flowed toward sample cell. This step was automatically achieved

under the control of the computer control software. At the end, the pressure, temperature, adsorption and other relevant data were stored in the computer system.

2.3 Total organic carbon

The non-dispersive infrared absorption method was carried out to quantify the total organic carbon (TOC) of given sample and following steps followed: (1) preparation, (2) inorganic carbon treatment, (3) cleaning after acid solution treatment, (4) testing and (5) data processing. At the end, following equation was used to get the TOC of given samples:

$$\text{TOC} = \frac{m_3 - m_1}{m_2} \times \text{TOC}_o \quad (1)$$

where m_1 , m_2 and m_3 are an experiment recorded mass, pre-processing sample quality mass, and post-processing sample and the crucible mass, respectively, g and TOC_o is the tested TOC, wt%.

3 Mathematical model and validation

3.1 Gas sorption-induced pore radius change

Langmuir is one of the important and common model through which gas sorption can be quantified using below equation [20]:

$$V_a = V_L \frac{P}{P_L + P} \quad (2)$$

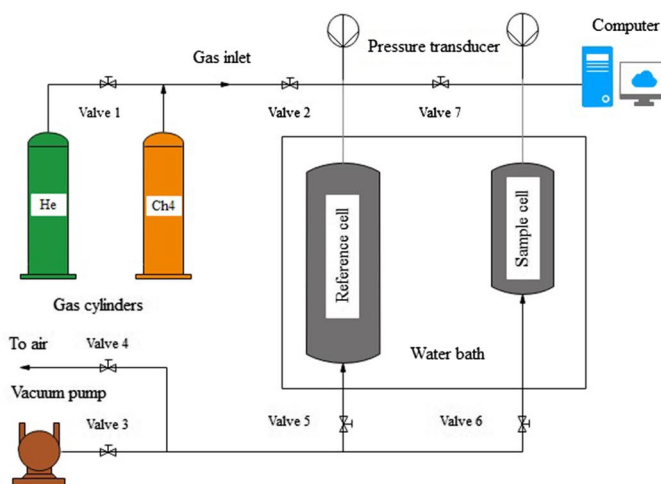


Fig. 1 Schematic diagram of isotherm gas sorption equipment

where V_a and V_L is the absolute gas sorption and Langmuir volume, mmol/g and P and P_L is the equilibrium gas and Langmuir pressure, MPa. The existence of adsorbed gas in shale alters the effective pore size and affects the gas transport phenomena. The effective pore radius can be defined as [22]:

$$r_p = r_o - \Delta r \tag{3}$$

where r_p , r_o and Δr is the effective pore radius, actual pore radius and pore thickness, m . According to the Langmuir model, the above Eq. (3) can be expressed in term of average pore radius measurement as [7]:

$$r_p = r_o - \theta d_m \tag{4}$$

where d_m is the diameter of gas molecule, and θ is the gas coverage which can be measured as:

$$\theta = \frac{P}{P_L + P} \tag{5}$$

Dubinin–Radushkevich (DR) proposed gas sorption model-based on a pore-filling mechanism and expressed as [34, 46]:

$$V_a = V_o \cdot \exp \left[-D \cdot \left\{ \ln \left(\frac{\rho_{ads}}{\rho_g} \right) \right\}^2 \right] \tag{6}$$

where V_a and V_o is the gas sorption and maximum gas sorption, mmol/g; D is the parameter related to the affinity of the sorbent for the gas, and ρ_{ads} and ρ_g is the adsorbed and free gas density; kg/m³. According to above model, the Eq. (3) can also be expressed as:

$$r_p = r_o - \frac{V_a}{\rho_{ads}SSA} = r_o - \frac{V_o}{\rho_{ads}SSA} \exp \left[-D \cdot \left\{ \ln \left(\frac{\rho_{ads}}{\rho_g} \right) \right\}^2 \right] \tag{7}$$

where SSA is the specific surface area, m²/g.

3.2 Gas apparent permeability model

Due to the presence of various flow regimes in SGR, Darcy’s law cannot provide the actual behavior of gases and its transport phenomena in nanopores. The flow regimes such as Darcy, slip, transition and free molecules can be identified on the basis of Knudsen number. The Knudsen number can be defined as [16].

$$K_{n1} = \frac{\lambda}{r_p} \tag{8}$$

where r_p is the pore radius, m and λ are the mean free path of gas molecules that can be defined as:

$$\lambda = \frac{K_b T}{\sqrt{2} \pi \delta_m^2 p} \tag{9}$$

where K_b is the Boltzmann constant, J/K ; T is the temperature, K ; δ_m is the diameter of gas molecule collision, m ; and p is the pressure, Pascal. In most of SGR the Knudsen number lies between 10⁻³ to 1 [42] which indicates that the slip and transition flow regimes are most likely encountered in such reservoirs. According to the Eqs. 4 and 7, the Knudsen number may also expressed as:

$$K_{n2} = \frac{\lambda}{r_o - \left(\frac{P}{P_L + P} \right) d_m} \tag{10}$$

$$K_{n3} = \frac{\lambda}{r_o - \frac{V_o}{\rho_{ads}SSA} \exp \left[-D \cdot \left\{ \ln \left(\frac{\rho_{ads}}{\rho_g} \right) \right\}^2 \right]} \tag{11}$$

The gas apparent permeability of SGR is generally relies on Knudsen number and absolute permeability and can be expressed as [35]:

$$K_{app} = k_a f(K_{ni}) \tag{12}$$

where k_a is the absolute permeability, mD, i term represents 1 or 2 or 3, and $f(k_{ni})$ is the slippage incremental term that can be expressed as:

$$f(K_{ni}) = (1 + \zeta K_{ni}) \left(1 + \frac{4K_{ni}}{1 - bK_{ni}} \right) \tag{13}$$

where b is the slip coefficient, and ζ is the dimensionless rarefaction coefficient that defined by [7] as:

$$\zeta = \frac{\zeta_o}{1 + \frac{A}{K_{ni}^B}} \tag{14}$$

where A , B and ζ_o are the constant terms and its value are 0.17, 0.4348 and 1.358, respectively. From literature, it was found that effective stress plays significant part in change of pore structure, absolute permeability and non-darcy flow in SGR. Dong et al. [11] proposed power law relation in between porosity and stress based on experiments and proposed following equation after some manipulation:

$$K_{app} = K_{a,i} \left(\frac{\sigma_m}{P_o} \right)^{-c\theta} \tag{15}$$

where $k_{a,o}$ is the absolute permeability under reference pressure (P_o), σ_m is the mean in-situ effective stress and C_φ is a dimensionless material-specific constant. Substitute the above equation in Eq. (12), we get Eq. (16) that

shows the combine impact of non-darcy/gas slippage and geomechanics into nanoflow behavior.

$$K_{app} = K_{a,o} \left(\frac{\sigma_m}{\rho_o} \right)^{-c\theta} f(K_{n1}) \tag{16}$$

It is worth noting that in a general porous media, the loss in cross section area is equivalent to the loss in porosity or permeability and it can be defined as:

$$\frac{\theta}{\theta_o} = \frac{r_p^2}{r_o^2} \tag{17}$$

$$\frac{K_a}{K_{a,o}} = \frac{r_p^2}{r_o^2} \tag{18}$$

Equation (16) can be modifying based on Eqs. (17) and (18) for account the impact of adsorbed layer on gas apparent permeability model as:

$$K_{app} = K_{a,o} \frac{\left[r_o \left(\frac{\sigma_m}{\sigma_{m,o}} \right)^{-c\theta} - d_m \left(\frac{p}{p_L + p} \right) \right]^2}{r_o^2} f(K_{n2}) \tag{19}$$

$$K_{app} = K_{a,o} \frac{\left[r_o \left(\frac{\sigma_m}{\sigma_{m,o}} \right)^{-c\theta} - \frac{V_o}{\rho_{abs} SSA} \left(-D \left[\ln \left(\frac{\rho_{ads}}{\rho_g} \right) \right]^2 \right) \right]^2}{r_o^2} f(K_{n3}) \tag{20}$$

The Eqs. (19) and (20) describe the combine effect of non-darcy/gas slippage, geomechanics and adsorbed layer into nanoflow behavior based on Langmuir and SDR models, respectively.

3.3 Model validation

The experimental data of gas permeability and gas adsorption for shale sample were taken from Zamirian et al. [43] and validated the proposed gas apparent permeability model. The gas permeability was measured through steady state technique at desired pore pressure, confining pressure and temperature by using carbon dioxide gas. The crushed sample having 1.2% total organic content (TOC) was used to measure the gas adsorption capacity of shale sample at temperature 40 °C. Our proposed gas apparent permeability model, which comprising non-darcy/gas slippage, geomechanics and adsorbed layer impact based on SDR model, is validated and found in good agreement with experimental data as compared to existing model which can be seen in Fig. 2.

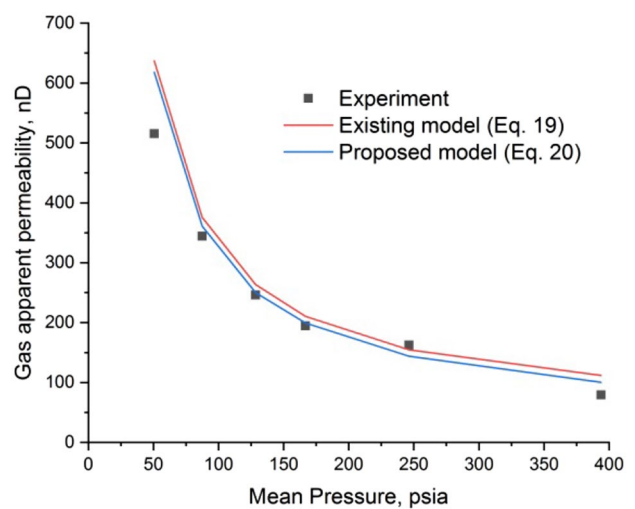


Fig. 2 Results of gas apparent permeability model validation

4 Results and discussion

4.1 Gas sorption-experiment and models

Gas sorption experiments on two shale samples were conducted and the experimental data fitted using Langmuir and SDR models. Then, the effective pore radius was analyzed based on these models. Gas sorption data from literature sources were also collected for comparison analysis. For measurement of Langmuir and SDR model fitting parameters the MATLAB curve fitting tool and ORIGIN tool box was used, respectively. The temperature, TOC and curve fitting parameters of this study and literature are shown in Table 1. It is worth noting that the initial pore radius was assumed as 12 nm and some important parameters from literature were also taken in this study (Table 2).

The Langmuir and SDR model were used in this study to fit the experiments data, and their results are shown in Fig. 3 results were obtained by fitting the experimental data using regression analysis tools as defined above. Both Langmuir and SDR model results can be seen in Fig. 3. Results show that SDR model has good fit to experimental data than Langmuir model as indicated by value of coefficient of determination (Table 1), and the similar results were also observed when using literature data (Fig. 4).

It was further observed in Fig. 4 that the Langmuir model provides poor results especially at high pressure and may underestimate the impacts of adsorbed layer thickness. Such poor result mostly seen when shale is rich in organic carbon [25]. On other hand, the SDR model is best suited as it based on micropore-filling mechanism and is providing better results than Langmuir model at both low as well as high pressure. In addition, the gas adsorption is largely influenced by low to high pressure

Table 1 TOC and curve fitting parameters of shale samples

ID	Temp, K	TOC, wt%	Langmuir model-based			SDR model-based				References
			V_L , mmol/g	P_L , MPa	R^2	V_{or} , mmol/g	ρ_{ads} , kg/m ³	D	R^2	
3-124	318.15	3.66	0.176	2.266	0.990	0.1746	520.810	0.0559	0.996	This study
3-153	318.15	2.94	0.191	6.431	0.999	0.1555	374.622	0.1061	0.999	
S-B	383.15	4.76	0.353	2.362	0.991	0.3445	353.169	0.0725	0.999	Chen et al. [4]
HY-10	328.15	0.14	0.106	6.84	0.998	0.0886	279.675	0.1377	0.986	Hou et al. [14]
X2-2	333.15	5.3	0.149	1.714	0.993	0.1564	319.998	0.0634	0.998	Zhou et al. [44]
X3-3	333.15	3.7	0.068	0.820	0.799	0.0885	271.381	0.0652	0.998	
105-1	423.15	1.9	0.123	3.033	0.980	0.1358	251.425	0.0959	0.999	Zhou et al. [47]
105-15	423.15	2.4	0.198	2.756	0.994	0.2087	286.825	0.0778	0.999	

Table 2 Some important parameters used in calculations

Parameters	Value	References
Boltzmann constant, J/K	1.38E-23	Javadpour [16]
Dimensionless material-specific constant	0.035	Wang et al. [3]
Pressure at reference condition, MPa	0.1	Wang et al. [3]
Collision diameter of methane gas molecules, nm	0.38	Rasoul [33]
Density of adsorbed gas phase, g/cm ³	0.34	Ambrose et al. [1]
Slip coefficient	-1	Beskok, Karniadakis [2]

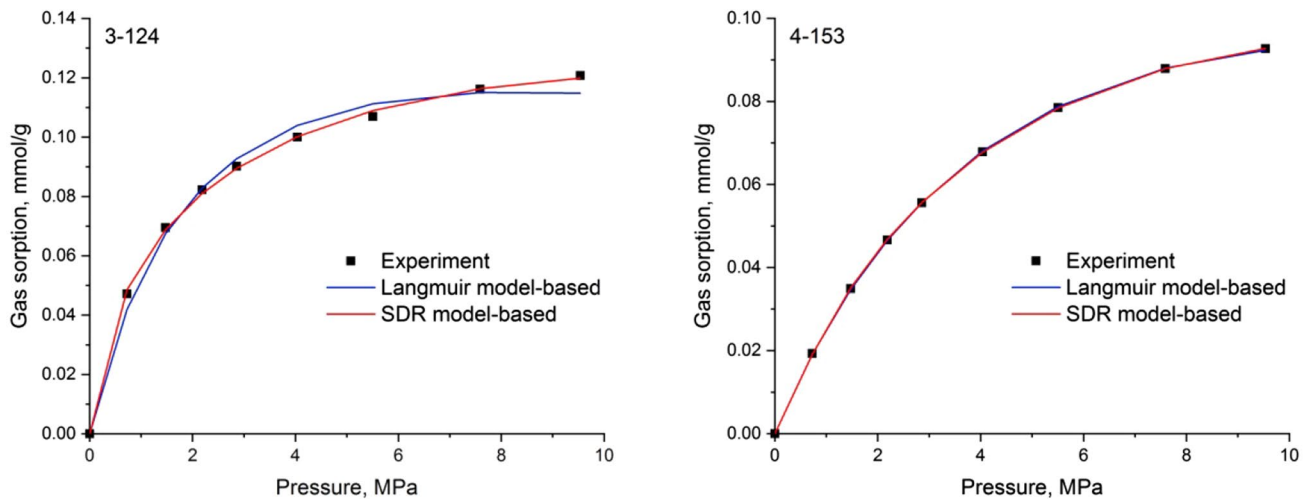


Fig. 3 Experimental and model results of gas sorption for this study

changes and its curve increases as pore pressure increases, but in some samples, its curve increases until it reaches a maximum value and afterward its curve falls continuously. Such curve decline might be due to different physical properties, i.e., organic matter content, pore structure, surface area etc.

4.2 Impact of adsorbed phase gas density on gas sorption

Previous studies assumed various densities of adsorbed gas phase (ρ_{ads}) values in their studies, i.e., 0.34 g/cm³ [1], 0.421 g/cm³ [5, 40], 0.210–0.546 g/cm³ [20]. From these literatures, it was observed that density of adsorbed gas

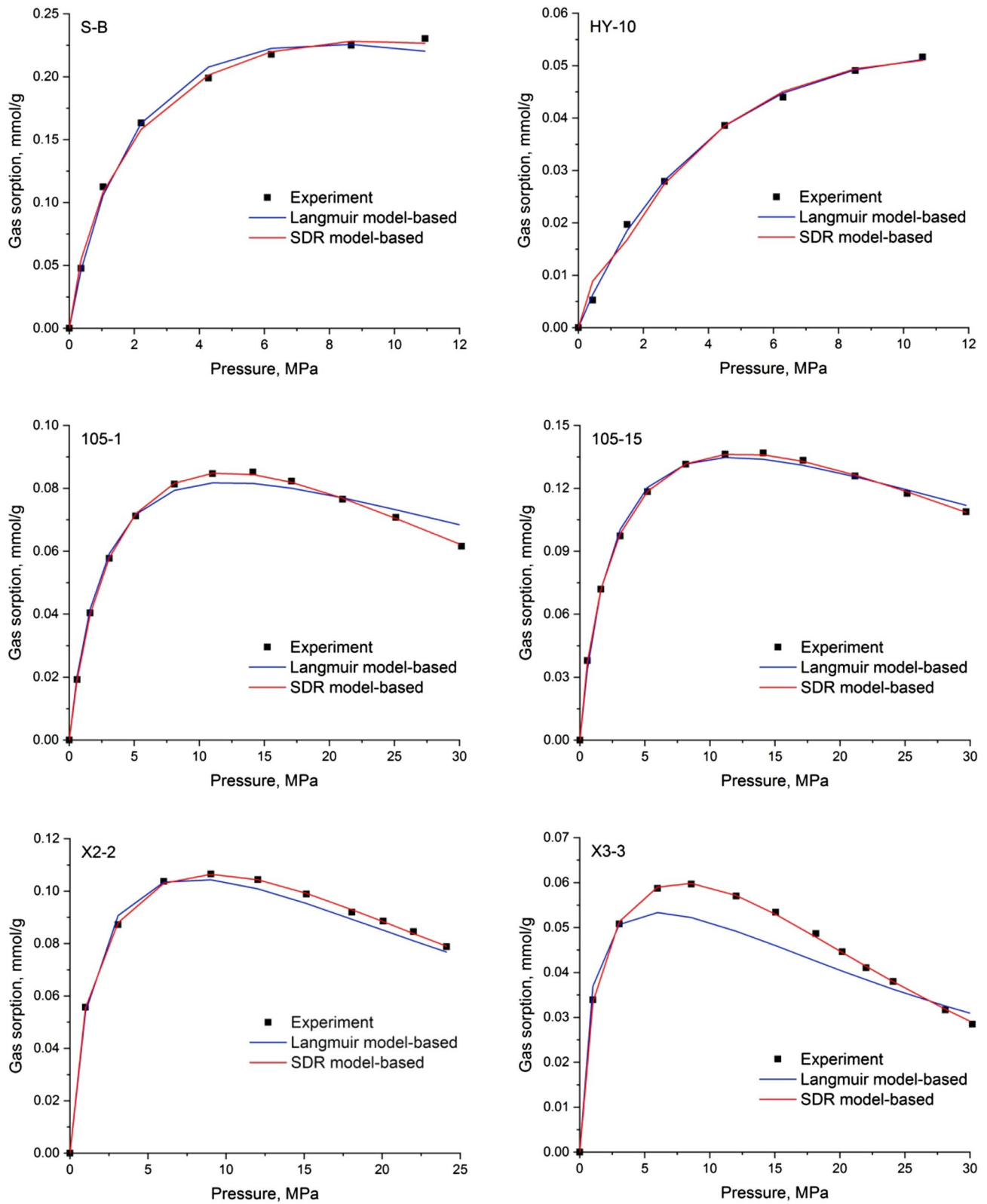


Fig. 4 Experimental and model results of gas sorption for literature study

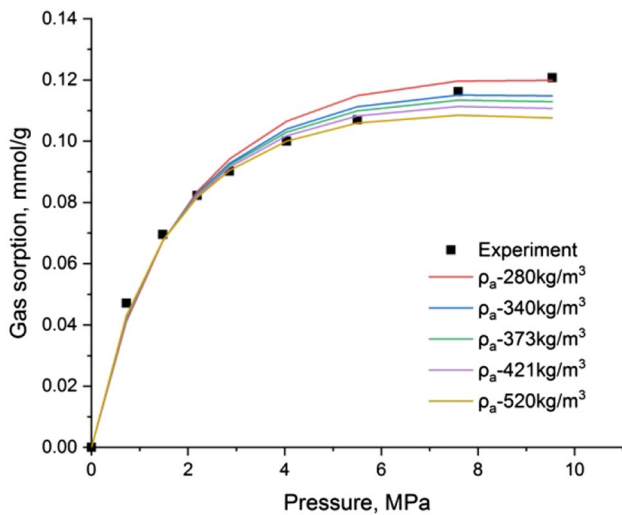


Fig. 5 Impact of adsorbed phase gas density on gas sorption for sample 3-124

phase is a key factor and plays a vital role in gas sorption measurement. The gas sorption capacity is usually

increasing with decrease in adsorbed gas phase density and that can be seen in Fig. 5. Hence, accurate measurement of adsorbed gas phase density is essential for shale gas characterization and assessment.

4.3 Impact of gas sorption on adsorbed layer thickness of pore radius

It was observed in Fig. 6 that the gas sorption increases as pressure increases, but on other hand, the effective pore radius decreases as pressure increases. The increasing rate of gas sorption was observed to vary in each sample as it depends on shale properties and characteristics. In addition, pore radius was affected by gas sorption and its affecting rate was also found to vary. For example, the pore radius of sample 3-124 was more affected than sample 4-153. The main reason might be sample 3-124 have high gas sorption capacity due to high TOC content than sample 4-153. The variation in results of effective pore radius was also observed when using Langmuir and SDR models. It was further observed that the effective pore

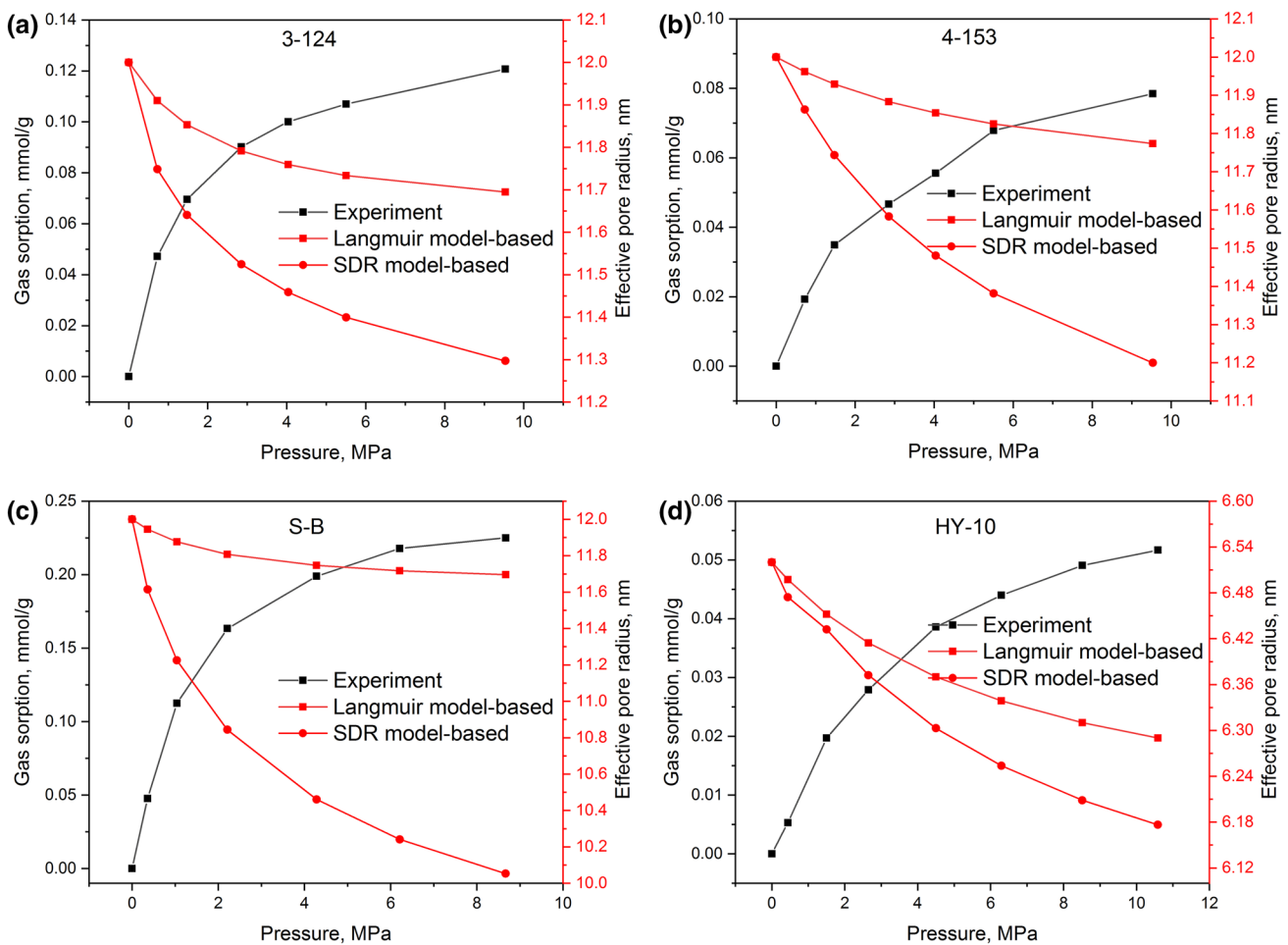


Fig. 6 Gas sorption and effective pore radius of shale samples **a** 3-124, **b** 4-153, **c** S-B and **d** HY-10

radius measured through SDR model followed the same alteration as gas sorption at same pressure as compared to Langmuir model. For example, the behavior of gas sorption in sample HY-10 was altered from 0 to 2 MPa and at same pressure the effective pore radius-based SDR model was also altered, but no alteration was found on effective pore radius-based Langmuir model. Similar results were also observed in literature. Hence, such findings show that effective pore radius-based SDR model may provide more accurate measurement than Langmuir based.

Moreover, effective pore radius was also investigated at high pressure and it was observed that the effective pore radius was more reduced at SDR model than Langmuir model, and the reduction rate of effective pore radius was varying in each shale samples (Fig. 7).

The gas sorption-induced swelling and pore shrinkage also play dominant role in shale. These both study are very

broad and might be more sophisticated at effective stress. The physical properties, such as porosity, permeability are greatly influence due to these factors. Furthermore, the pore and confining pressures act to compress the samples. Accordingly, these effects are deducted from the strain measurements to estimate the swelling due to gas sorption. In our study, we have used crushed samples so it is not possible to apply confining pressures which act as compress the samples and then to measure the gas sorption-induced swelling. The intact core sample and other equipment are to be required to conduct such study. That is why we have not included the impact of gas adsorption-induced swelling/pore shrinkage in our study.

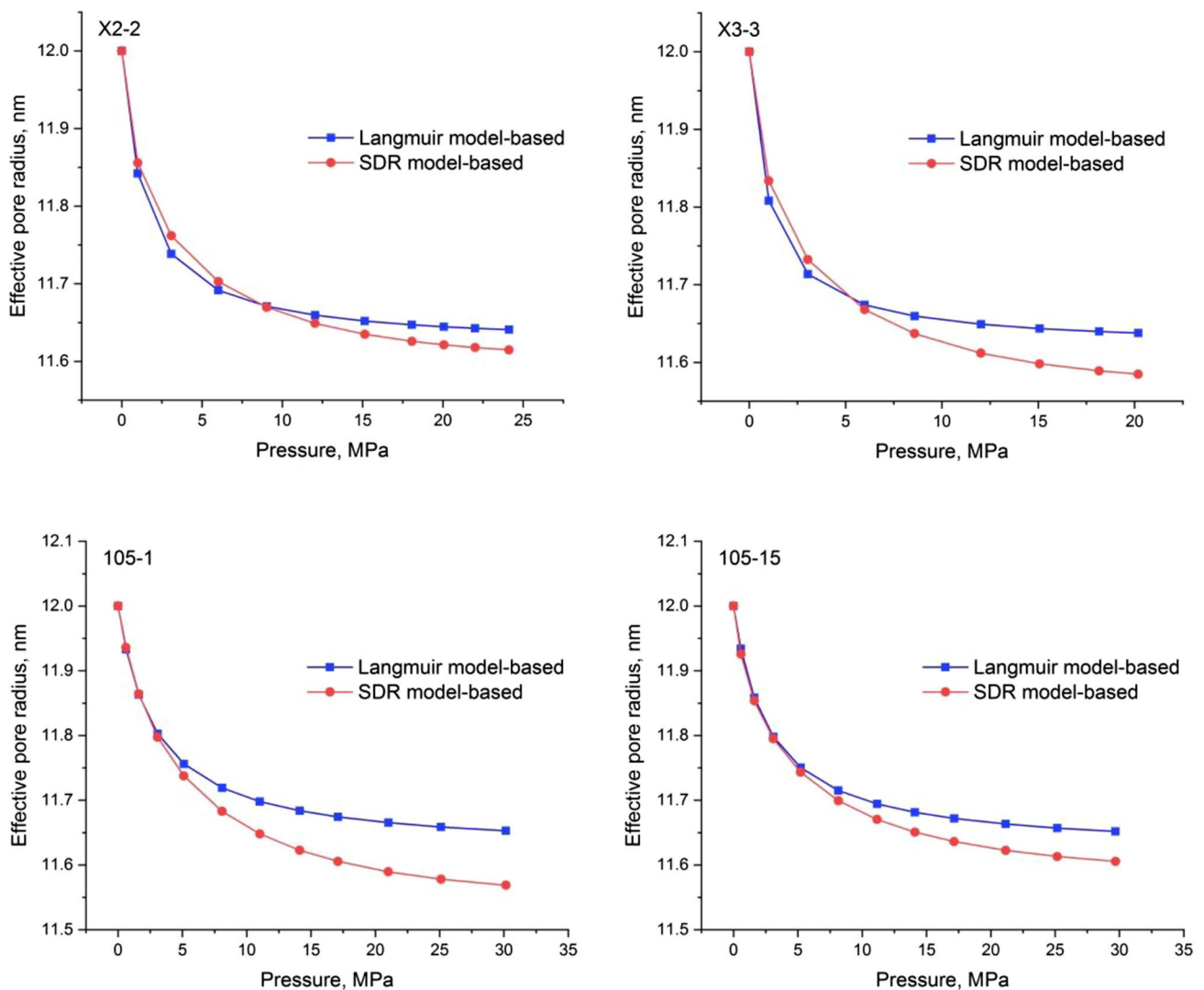


Fig. 7 Gas sorption-induced pore radius change of shale samples

4.4 Impact of main controlling factors of shale on pore radius

It was observed in this study that the average pore radius impacts on different shale samples vary and this might be controlling factors of gas sorption such as TOC and SSA, existence of organic matter and mineral components and pore structure characteristics. The gas sorption capacity mostly increases with TOC increase, whereas no uniform relation in between the gas sorption capacity and SSA was found. In addition, both TOC and SSA are the controlling factors of gas sorption capacity. The different shale samples have different SSA and gas sorption capacity whereas such factors may vary due to the presence of kerogen type and mineral components as well as in SGR. In addition, pore structure also reflects the gas sorption mechanisms. Keeping view on above factors, the following main findings were also observed in this study; (a) the reduction of pore radius and its thickness may vary and this might be due to gas sorption factors change such as TOC, SSA, etc. (b) pore structure plays a crucial role in pore radius reduction as different nanopore structures reflect the gas sorption mechanisms. Zhou et al. [47] showed that the mesopores are more controlled by shale than micropores and providing more than 50% total SSA than micro-SSA's and same results was found in this study. For example, Sample Y-105-1 and Y-105-15 have contributed micro-SSA's about 42.96% and 42.72% whereas meso-SSA's about 57.04% and 57.28%, respectively, and (c) organic matter and mineral components also affect pore radius as different shale sample containing different SSA in mineral components [21] and [12]. For example, SSA of Kerogen-isolated is 161.23 m²/g in Niutitang shales [18], whereas 193.1 m²/g is in Longmaxi shales [3].

4.5 Impact of pore radius on gas apparent permeability

As observed above that the gas apparent permeability relies on Knudsen number and absolute permeability, whereas the Knudsen number is affected by gas sorption-induced pore radius; hence, correction in Knudsen number must be made prior to gas apparent permeability measurement. The non-darcy/gas slippage, geomechanics and adsorbed layer factors are impacts on gas apparent permeability; therefore, for investigation of such factors, the 4 cases were developed in this study and also corrected Knudsen number for accurate measurement of gas apparent permeability. The details of cases are shown in Table 3. It is noted that permeability data were obtained from Sinha et al. [32] for evolution of gas apparent permeability at different cases.

Table 3 Model cases used in this study

Cases	Details
Case-1	Only impact of gas slippage was considered
Case-2	Impact of gas slippage and geomechanics was considered
Case-3	Impact of gas slippage, geomechanics and adsorbed layer-based Langmuir model was considered
Case-4	Impact of gas slippage, geomechanics and adsorbed layer-based SDR model was considered

Result revealed from Fig. 8 that the gas apparent permeability may depend on shale properties at various pressures, temperatures and pore sizes and it decreases as pressure increases due to gas slippage, geomechanics and adsorbed layer impacts and also positively correlated with pore size change. The pore size decreases due to the presence of adsorption layer and affects the gas apparent permeability. The adsorption layer measured using Eqs. (4) and (7) provided different values and result change in gas apparent permeability at different models, i.e., Equations (19) and (20). The gas apparent permeability was decreased around 9.87 to 17.45% from pressure 115 to 1969 MPa at sample 3-124 when adsorbed layer-based Langmuir model (cases-3) was compared with case-1 and around 11.35 to 21.65% gas apparent permeability was decreased at same pressure when adsorbed layer-based SDR (cases-4) was compared with same case-1. Similarly, in sample 4-153, the gas apparent permeability was decreased around 9.40 to 16.28% when case-3 was compared with case-1 and around 10.31 to 21.88% when cases-4 was compared with case-1 at same pressure. The similar results were also observed in sample SB. Hence, it was concluded from these results that the gas apparent permeability was observed to be lower at adsorbed layer-based SDR model than adsorbed layer-based Langmuir model in this study and the similar results was also found in literature.

5 Conclusion

From this study it can be concluded that;

- The SDR model provided more accurate study of influence of gas sorption on pore radius and thickness, and accurate adsorbed gas phase density compared to the Langmuir model at both low and high pressures.
- The pore size was affected due to gas sorption-induced pore radius and result the gas apparent permeability was alter. In addition, it might more affect due to change of TOC, SSA, pore structure, organic matter and mineral components.

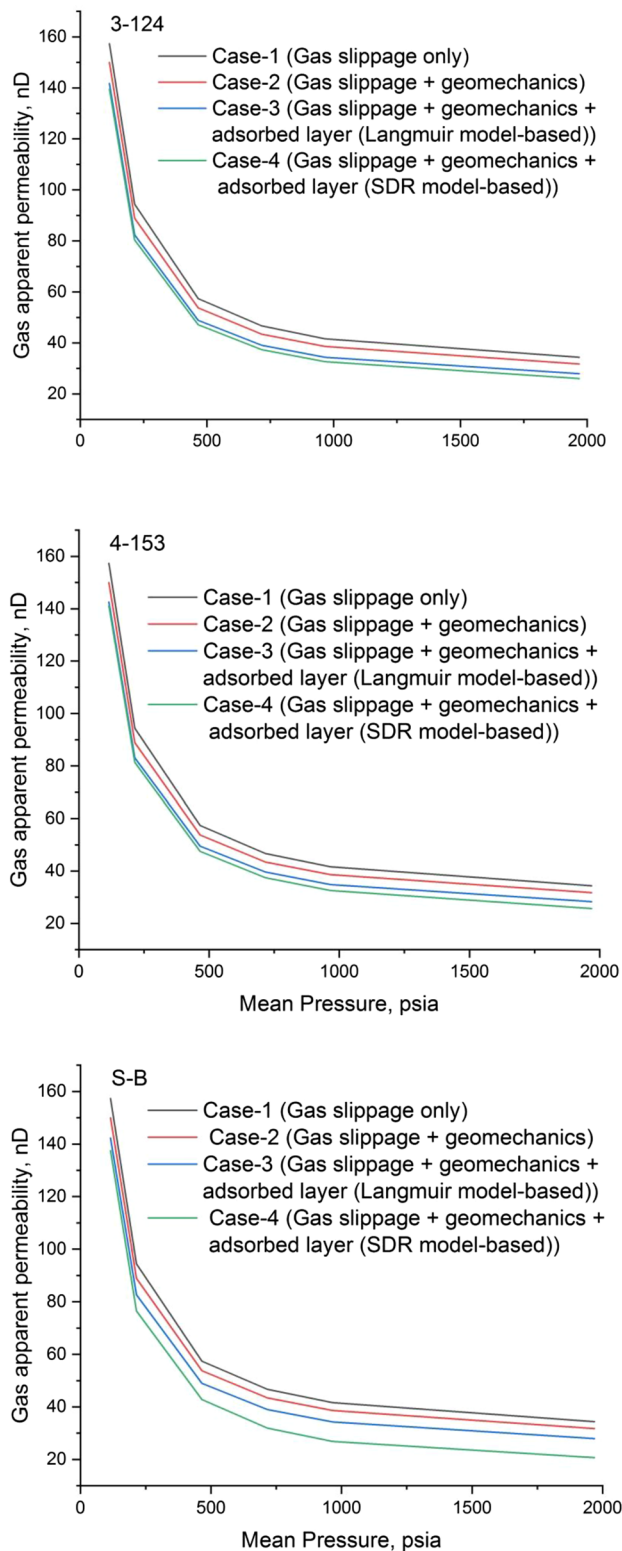


Fig. 8 Gas apparent permeability at different cases

- The Knudsen number was also affected due to gas sorption-induced pore radius change; thus, it was corrected for accurate measurement of gas apparent permeability.

- The gas apparent permeability was observed to lower at adsorbed layer-based on SDR model compared to Langmuir model.
- From evolution of gas apparent permeability at different cases, it was observed that the gas apparent permeability was decreased around 9.87–17.45% when case-3 compared with case-1 and around 11.35–21.65% when cases-4 compared with same case-1 from pressure 115 to 1969 MPa at sample 3-124. Similarly at sample 4-153, it was decreased around 9.40–16.28% when case-3 compared with case-1 and around 10.31–21.88% when cases-4 compared with same case-1 at same pressure. The similar results were also observed in S-B sample.

Acknowledgements This work was supported by the National Natural Science Foundation of China (NO.51774308), the National Science and Technology Major Project of China (2016ZX05014-003-002).

Compliance with ethical standards

Conflicts of interest We have no conflicts of interest to declare in this manuscript.

References

1. Ambrose RJ, Chad HR, Mery DC, Yucel AI, Carl, S (2010) New pore-scale considerations for shale gas in place calculations, presented at spe unconventional gas conference held in Pittsburgh, Pennsylvania, USA, 23–25 Feb 2010, (SPE 131772)
2. Beskok A, Karniadakis GE (1999) Report: a model for flows in channels, pipes, and ducts at micro and nano scales. *Microscale Thermophys Eng* 3:43–77
3. Cao T, Song Z, Wang S, Xia J (2015) A comparative study of the specific area and pore structure of different shales and their kerogens. *Sci China Press* 45(2):139–151
4. Chen L, Jinag Z, Liu Z, Ji W, Wang P, Gao F, Hu T (2017) Application of Langmuir and Dubinin-Radushkevich models to estimate methane sorption. *Energy Explor Exploit* 35(1):122–144
5. Chen L, Zuo L, Jiang Z, Jiang S, Liu K, Tan J, Zhang L (2019) Mechanisms of shale gas adsorption: evidence from thermodynamics and kinetics study of methane adsorption on shale. *Chem Eng J* 361:559–570
6. Chen Z, Pan Z, Liu J, Connell LD, Elsworth D (2011) Effect of the effective stress coefficient and sorption-induced strain on the evolution of coal permeability: experimental observations. *Int J Greenh Gas Control* 5:1284–1293
7. Civan F, Rai CS, Sondergeld CH (2011) Shale–gas permeability and diffusivity inferred by improved formulation of relevant retention and transport mechanisms. *Transp Porous Media* 86:925–944
8. Clarkson CR, Bustin RM, Levy JH (1997) Application of mono/multilayer and adsorption potential theories to coal methane isotherms at elevated temperature and pressure. *Carbon* 35(12):1689–1705
9. Cui X, Bustin AMM, Bustin RM (2009) Measurements of gas permeability and dif-fusivity of tight reservoir rocks: diff erent approaches and their applications. *Geofluids* 9(3):208–223

10. Darabi H, Ettehad A, Javadpour F, Sepehrnoori K (2012) Gas flow in ultra-tight shale strata. *J Fluid Mech* 710(12):641–658
11. Dong JJ, Hsu JY, Wu WJ (2010) Stress-dependence of the permeability and porosity of sandstone and shale from TCDP hole-A. *Int J Rock Mech Min Sci* 47(7):1141–1157
12. Fan E, Tang S, Zhang C, Guo Q, Sun C (2014) Methane sorption capacity of organics and clays in high-over matured shale-gas systems. *Energy Explore Exploit* 32(6):927–942
13. Guo C, Wei M, Liu H (2015) Modeling of gas production from shale reservoirs considering multiple transport mechanisms. *PLoS ONE* 10:e0143649
14. Hou Y, He S, Harris NB, Ji J, Wang J, Zhang J, Chunyang C (2017) The effects of shale composition and pore structure on gas adsorption potential in highly mature marine shales, Lower Paleozoic, central Yangtze, China. *Can J Earth Sci* 54:1033–1048
15. Huang S, Wu Y, Cheng L, Liu H, Xue Y, Ding G (2018) Apparent permeability model for shale gas reservoirs considering multiple transport mechanisms. *Geofluids* 18:1–18
16. Javadpour F (2009) Nanopores and apparent permeability of gas flow in mudrocks (shales and siltstone). *J Can Pet Technol* 48(8):16–21
17. Javadpour F, Fisher D, Unsworth M (2007) Nanoscale gas flow in shale gas sediments. *J Can Pet Technol* 46:55–61
18. Ji L, Zhang T, Milliken KL, Qu J, Zhang X (2012) Experimental investigation of main controls to methane adsorption in clay-rich rocks. *Appl Geochem* 27(12):2533–2545
19. Kang SM, Fathi E, Ambrose RJ, Akkutlu IY, Sigal RF (2011) Carbon dioxide storage capacity of organic-rich shales. *SPE J* 16(4):842–855
20. Li J, Zhou S, Gaus G, Li Y, Ma Y, Chen K, Zhang Y (2018) Characterization of methane adsorption on shale and isolated kerogen from the Sichuan Basin under pressure up to 60 MPa: experimental results and geological implications. *Int J Coal Geol* 189:83–93
21. Liu D, Yuan P, Liu H, Li T, Tan D, Yuan W (2013) High-pressure adsorption of methane on montmorillonite, kaolinite and illite. *Appl Clay Sci* 85:25–30
22. Memon A, Li A, Han W, Tian W (2019) Effect of gas adsorption-induced pore radius and effective stress on shale gas permeability in slip flow: new insights. *Open Geosci* 11(1):948–960
23. Memon A, Li A, Jacqueline N, Kashif Ma M (2020) Study of gas sorption, stress effects and analysis of effective porosity and permeability for shale gas reservoirs. *J Pet Sci Eng* 193:107370
24. Memon A, Li A, Muther T, Ren X (2020) An experimental study of gas sorption, adsorbed and sorbed porosity and their impact on shale gas-in-place calculations. *J Porous Media* 23(10):985–1000
25. Memon A, Li A, Memon BS, Muther T, Wencheng H, Kashif M, Tahir MU, Akbar I (2020c) Gas adsorption and controlling factors of shale: review, application, comparison and challenges. *Nat Resour Res* 1–22
26. Moghaddam RN, Jamiolahmady M (2016) Slip flow in porous media. *Fuel* 173:298–310
27. Passey QR, Bohacs K, Esch WL (2010) From oil-prone source rock to gas-producing shale reservoir-geologic and petrophysical characterization of unconventional shale gas reservoirs. International oil and gas conference and exhibition in China, 8–10 June 2010 (SPE-131350)
28. Sakhaee-pour A, Bryant SL (2011) Gas permeability of shale. Society of Petroleum Engineers, (146944-MS)
29. Sakurovs R, Day S, Weir S (2010) Relationships between the critical properties of gases and their high pressure sorption behavior on coals. *Energy Fuels* 24:1781–1787
30. Sigal RF, Akkutlu IY, Kang SM, Diaz-Campos M, Ambrose R (2013) The laboratory measurement of the gas storage capacity organic shales. *Petrophysics* 54:224–235
31. Singh H, Javadpour F, Ettehadtavakkol A, Darabi H (2013) Non-empirical apparent permeability of shale. *SPE Reserv Eval Eng* 17(3):414–424
32. Sinha S, Braun EM, Passey QR, Onardi SA, Boros JA, Wood AC, Zirkle T, Kudva RA (2013) Steady-state permeability measurements on intact shale samples at reservoir conditions-effect of stress, temperature, pressure, and type of gas, presented at middle east oil and gas show and conference for the society of petroleum engineers, Manama, Bahrain, 10–13 Mar 2013
33. Rasoul NM, Mahmoud J (2016) Fluid transport in shale gas reservoirs: simultaneous effects of stress and slippage on matrix permeability. *Int J Coal Geol* 163:87–99
34. Tian H, Li T, Zhang T, Xiao X (2016) Characterization of methane adsorption on over-mature Lower Silurian–Upper Ordovician shales in Sichuan Basin southwest China: experimental results and geological implications. *Int J Coal Geol* 156:36–49
35. Wang H, Porcu MM (2016) Impact of shale-gas apparent permeability on production: combined effects of non-darcy flow/gas-slippage, desorption, and geomechanics. *SPE Reserv Eval Eng* 18(04):495–507
36. Wei M, Liu J, Elsworth D, Wang E (2018) Triple-porosity modeling for the simulation of multiscale flow mechanisms in shale reservoirs. *Geofluids* 18:1–11
37. Wei M, Liu J, Feng X, Wang C, Zhou F (2016) Evolution of shale apparent permeability from stress-controlled to displacement-controlled conditions. *J Nat Gas Sci Eng* 34:1453–1460
38. Wu K, Chen Z, Li X, Guo C, Wei M (2016) A model for multiple transport mechanisms through nanopores of shale gas reservoirs with real gas effect-adsorption-mechanic coupling. *Int J Heat Mass Transf* 93:408–426
39. Xiong J, Liu X, Liang L, Zeng Q (2017) Adsorption of methane in organic-rich shale nanopores: an experimental and molecular simulation study. *Fuel* 200:299–315
40. Yang T, Li X, Zhang Z (2015) Quantitative dynamic analysis of gas desorption contribution to production in shale gas reservoirs. *J Unconv Oil Gas Resour* 9:18–30
41. Yu W, Sepehrnoori K, Patzek TW (2014) Evaluation of gas adsorption in Marcellus shale. In: SPE annual technical conference and exhibition. Amsterdam, The Netherlands, 2014 (SPE-170801)
42. Ziarani AS, Aguilera R (2011) Knudsen's permeability correction for tight porous media. *Transp Porous Media* 91(1):239–260
43. Zamirian M, Aminian K, Fathi E, Ameri S (2014) A fast and robust technique for accurate measurement of the organic-rich shales characteristics under steady-state conditions. *Soc Pet Eng*
44. Zhou S, Xue H, Ning Y, Guo W, Zhang Q (2018) Experimental study of supercritical methane adsorption in Longmaxi shale: insights into the density of adsorbed methane. *Fuel* 211:140–148
45. Zhang Q, Su Y, Wang W, Lu M, Sheng G (2017) Apparent permeability for liquid transport in nanopores of shale reservoirs: coupling flow enhancement and near wall flow. *Int J Heat Mass Transf* 115:224–234
46. Zhao T, Li X, Zhao H, Dou X (2015) Micro-storage state and adsorption behavior of shale gas, presented at nigeria annual international conference and exhibition for the society of petroleum engineers, Lagos, Nigeria, 4–6 Aug 2015
47. Zhou S, Honglin S, Chen H, Wang H, Guo W, Liu D, Zhang Q, Wu J, Shen W (2019) A comparative study of the nanopore structure characteristics of coals and Longmaxi shales in China. *Energy Sci Eng* 7(6):2050–505

Publisher's Note Springer Nature remains neutral with regard to jurisdictional claims in published maps and institutional affiliations.